Bone 124 (2019) 103–117

Contents lists available at ScienceDirect

Bone

journal homepage: www.elsevier.com/locate/bone

Full Length Article

Triple-threat activity of PEDF in bone tumors: Tumor inhibition, tissue preservation and cardioprotection against doxorubicin

Yongzhong Wei[a], Mina Elahy[b], Anna M. Friedhuber[c], Jia Y. Wong[d], Jeffery D. Hughes[d], Michael R. Doschak[e,f], Crispin R. Dass[d,g,h,*]

[a] Department of Orthopaedics, the First Affiliated Hospital with Nanjing Medical University, Nanjing 210029, China
[b] School of Medical Sciences, University of New South Wales, Kensington, Sydney, NSW 2052, Australia
[c] Department of Pathology, University of Melbourne, Parkville, Melbourne, VIC 3050, Australia
[d] School of Pharmacy and Biomedical Science, Curtin University, Bentley, Perth, WA 6102, Australia
[e] Department of Biomedical Engineering, University of Alberta, Alberta T6G 2E1, Canada
[f] Department of Dentistry, University of Alberta, Alberta T6G 2E1, Canada
[g] Curtin Health Innovation Research Institute, Curtin University, Bentley, Perth, WA 6102, Australia
[h] College of Health and Biomedicine, Victoria University, St Albans, Melbourne, VIC 3021, Australia

ARTICLE INFO

Keywords:
PEDF
Cancer
Bone
Doxorubicin
Metastasis

ABSTRACT

Pigment epithelium-derived factor (PEDF) is known for its osteogenic properties, but its effects against primary and secondary bone tumors have not comprehensively been demonstrated. We show the ubiquitous expression of PEDF in murine embryonic tissue. Continuous administration of PEDF in pregnant mice for five days did not adversely affect foetal health, despite PEDF's known potent antiangiogenic properties. In the case of the devastating childhood bone cancer osteosarcoma, PEDF has direct anticancer activity *per se*, and protects against the toxicity of doxorubicin in the heart, small intestine and testes. PEDF demonstrated anti-proliferative and pro-apoptotic effects against human prostate and breast cancer cells, tumors which are known to metastasize to bone as the preferred secondary site. Caspase-2 was activated in both tumor cell types by PEDF. In models of prostate and breast cancer in bone, PEDF significantly reduced tumor volumes. When combined with zoledronic acid, continuously-administered PEDF significantly reduced breast tumor volume at the bone, and was able to preserve the quality of bone better than the combination therapy. These multiple positive findings make PEDF an ideal endogenous and safe biological for possible future clinical testing.

1. Introduction

Bone is the most frequent site of metastasis in breast cancer, causing osteolytic or osteosclerotic changes, with subsequent pain and risk of pathological fractures, which may require surgical intervention [1]. Involvement of both the axial and appendicular skeleton commonly results in pain requiring analgesia and radiation therapy, and frequently contributes to debilitating symptoms prior to death [2]. To achieve secondary growth in bone, breast cancer cells invade the newfound matrix in bone *via* recruitment of osteoclasts, a class of cells responsible for resorbing bone mineral [3]. In addition, breast cancer cells are capable of invading the collagen I-rich matrix of bone *via* upregulation of collagenases such as MT1-MMP (membrane type 1 matrix metalloproteinase, also called MMP-14) [4]. MT1-MMP enhances collagen I fibril breakdown and phagocytosis [4,5]. Therefore, agents that can inhibit the production of osteoclasts (osteoclastogenesis) and downregulate MT1-MMP are likely to interfere with metastasis to bone.

One such promising protein is pigment epithelium-derived factor (PEDF), which possesses evolutionary-diversified roles that include the regulation of angiogenesis [6], neural stem cell survival and differentiation [7,8], antioxidant function in the eye [9], pro-differentiation in the bone [10,11], and growth inhibition in a variety of cancers [12]. PEDF is downregulated in breast cancer patients [13]. Of note, PEDF has a high affinity binding site for collagen I [14], the major protein found in bone, as well as glycosaminoglycans (GAGs) such as heparin and hyaluronan, which play important roles in bone formation [15,16]. We have further demonstrated that PEDF downregulates MT1-MMP expression in a variety of cancer cells [17,18] including the ER^- breast cancer cell line MDA-MB231 [17]. Osteoclasts play a dominant role in breast cancer metastases to bone [3]. The human ER^+ breast cancer cell line MCF-7 secretes receptor activator of nuclear factor κB ligand

* Corresponding author at: School of Pharmacy and Biomedical Science, Curtin University, GPO Box U1987, Perth 6845, Australia.
E-mail address: Crispin.Dass@curtin.edu.au (C.R. Dass).

https://doi.org/10.1016/j.bone.2019.04.014
Received 29 November 2018; Received in revised form 20 April 2019; Accepted 23 April 2019
Available online 24 April 2019
8756-3282/

(RANKL), which promotes osteoclastogenesis and subsequent bone mineral resorption [19]. RANKL and receptor activator of nuclear factor κB (RANK) are expressed by mammary epithelial cells under the control of sex hormones, and RANK and RANKL control the preferential metastasis of breast cancer cells to the bone [20]. We demonstrated that PEDF downregulates osteoclast differentiation, survival and activity *via* upregulation of osteoprotegerin (OPG), a decoy for RANKL [21].

While its role in osteogenesis is now well known, the role of PEDF in control of tumor cells that either originate from bone or metastasize towards it has largely been overlooked. It has been more than a decade since our lab first established the beneficial effects of PEDF against osteosarcoma (OS) [10,22,23]. OS is a primary malignant bone tumor with peak incidence in the second decade of life. A worldwide incidence of OS is about 3.4 per million people per year [24]. Eighty percent of cases are located in the metaphysis of long bones. Breast cancer is the second most common cancer diagnosed worldwide, affecting approximately one in eight women during their lifetime [25]. It has been estimated that between 20 and 30% of breast cancer patients will develop metastases, with bone being the predominant site [26]. Metastatic bone lesions that form as part of breast cancer are predominantly osteolytic, sometimes with pathological fracture. A similar predisposition to bone is also true for prostate cancer [27], the second most common cancer afflicting men [28].

Present therapies for bone metastases from breast cancer include the anti-RANKL monoclonal antibody, denosumab, and bisphosphonates such as zoledronic acid (ZA), which are also used against OS-mediated bone degradation. In a recent large-scale study, ZA improved invasive breast cancer disease-free survival in those who were over 5 years postmenopause at trial entry ($n = 1041$) but not in premenopausal or perimenopausal patients [29]. Denosumab has been found to be superior to ZA in delaying or preventing breast cancer-mediated skeletal-related events and alleviating pain [30]. Bisphosphonates and denosumab are associated with renal dysfunction, osteonecrosis of the jaw and hypocalcaemia [31]. PEDF may offer patients a safer alternative. PEDF administered continuously (2 weeks) *via* osmotic pumps did not alter serum creatinine, alkaline phosphatase and aspartate transaminase [32], though its effects on physiological angiogenesis have not been directly tested.

In this study, we demonstrate that PEDF is expressed ubiquitously in murine embryonic tissues and that it does not perturb physiological angiogenesis. However, it decreased the acidophilic basal zone of the secretory acini in pancreas. We demonstrate the anticancer effects of PEDF on other sarcoma cells such as liposarcoma and chondrosarcoma and lack of it in colorectal cancer cells. Not only is PEDF able to control osteosarcoma growth *in vivo* better than the frontline drug doxorubicin (Dox), it can mitigate the side-effects of Dox on tissues such as the heart, small intestine and skin. PEDF-mediated apoptosis in osteotropic prostate and breast cancer cells involved activation of caspase-2. When premixed with these classes of tumor cells and then injected orthotopically into bone, PEDF was able to significantly reduce tumor growth. When PEDF was combined with the anti-osteoclast drug ZA, it was more efficacious against breast tumor growth than either molecule administered alone. However, PEDF administered alone rendered better bone quality amongst all groups. These results point to the beneficial effects of PEDF against both primary bone and secondary (osteotropic) cancers.

2. Results

2.1. Expression and safety of PEDF in the developing murine foetus

PEDF was ubiquitously present in all foetal tissues examined (Fig. 1). Of note was expression seen in the cranial and digital sections, particularly within the chondrocytes. Intense expression was noted in the developing villi of the intestine, in the cytoplasm of both parietal and chief cells of the stomach, the glomeruli, the developing alveoli and connective tissue cells, the lymphoid precursor cells of the spleen, the red blood and erythroid cells present in the liver, very intense staining in brain cells including the neurons, at the back of the eye specifically the retina, in the corneal cells, and in the epidermis and subdermis of the developing skin, but not in the subaceous layer of the skin.

As foetal development relies heavily on angiogenesis and rapid cell division, growth and turnover, an *in utero* study was performed where PEDF or albumin was administered continuously for five days to pregnant mice starting at E5. Visibly, foetuses looked healthy in all groups when the amniotic sacs were gently exteriorized. There were no differences in the number of foetuses per mother in each treatment group (Fig. 2a), in the average foetal length (Fig. 2b) and in maternal inguinal fatpad width (unstretched, relaxed) between groups (Fig. 2c). We shifted attention to maternal weights and there was no difference between cohorts (Fig. 2d). During pregnancy, bone tissue turns over much more rapidly than in an age-matched non-pregnant female [33], with increasing foetal demands on maternal calcium repositories, the main target being bone. Thus, if PEDF has an untoward effect on maternal bone turnover, we would be able to detect it with microCT, but this was not the case as assessed on trabeculae bone volume in the maternal femur (Fig. 2e).

Upon histological staining, it was revealed that PEDF had no impact on trophoblast giant cells in the placenta (Fig. 2f, i-iii). Blood supply mostly *via* lacunae in the space between maternal and foetal vasculatures were clearly visible in all groups (Fig. 2f, iv-vi). In pancreatic tissues of pregnant mice, there was a discernible decrease in the acidophilic basal zone of the secretory acini (Fig. 2g, i-iii). There was no visible difference in the islets of Langerhans or in the number and shape of the secretory acini. There were no differences in adipose (inguinal fatpad; Fig. 2g, iv-vi) and muscle (gastrocnemius; Fig. 2g, vii-ix) tissues between the cohorts. We also examined that normal behavior such as grooming and maternal instincts such as nest-building were not altered, neither was social behavior such as interaction with other cage mates and degree of alertness to handling, nor was eating and drinking upon PEDF administration. Time taken for sutures to heal was also similar between the cohorts, with no visible difference in the visible appearance of the wound closure.

PEDF is more efficacious than Dox in an orthotopic murine model of osteosarcoma and acts as a chemoprotective against Dox in the heart and testis.

For the primary bone sarcoma osteosarcoma, it is not the prevalence that impacts greatly on society, but the devastating effect the cancer has on those in the prime of their lives – pre-teenagers to adolescents [34]. Fig. 3a shows that PEDF and Dox treatments did not have significant effect on the weight of mice across the treatment cohorts. Fig. 3b demonstrates that one-third of the mice in the control group developed 143B tumors. Dox inhibited the growth of tumors, hence, only 17% of the mice developed osteosarcoma. PEDF, on its own, provides a better antitumor effect than Dox evidenced by the fact that a mere 8% of the mice in this cohort bearing tumors, with the combination of PEDF and Dox showing lesser protection with 25% of the mice having tumors. Fig. 3c shows images of a representative mouse from each group. Tumors were quite aggressive in the combination group with extensive invasion of surrounding muscle tissue by the osteosarcoma cells (Fig. 3d). PEDF showed chemoprotective effects in not only the heart (Fig. 3e and f), but the small intestine (Fig. 3g and h) and the testis (Fig. 3i and j). In the heart, lesser degree of cellular vacuolation was noted in the Dox + PEDF group. In the small intestine, PEDF substantially reduced the number and size of hyperplastic spots around the base of the crypts. The clearest difference was seen in the testis, where inclusion of PEDF with Dox restored the tissue architecture near the centre of the seminiferous tubules. Follicular disruption in the skin (Fig. 3k) and perturbed vascularization in adipose tissue (Fig. 3l) were noted when animals were administered Dox, both being reduced by PEDF.

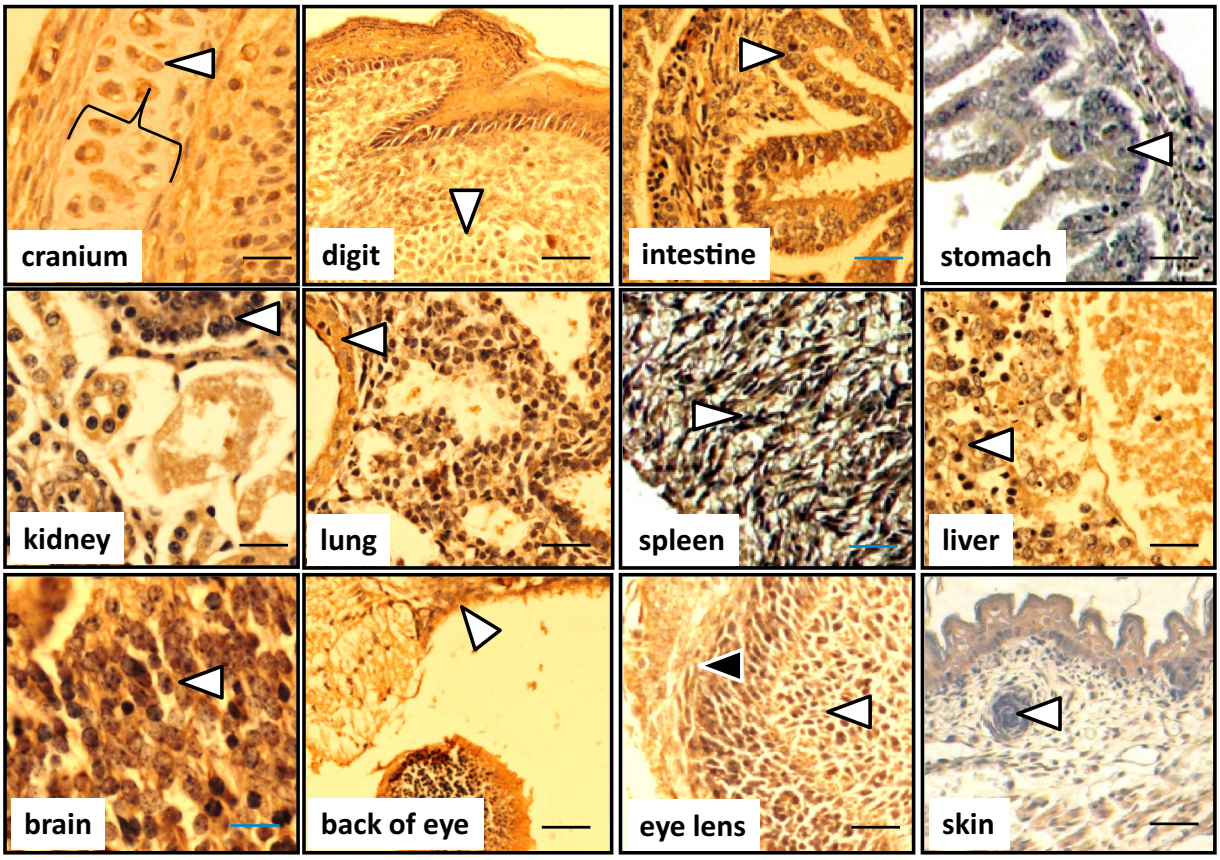

Fig. 1. Expression of PEDF in various foetal mouse tissues.
Tissues were harvested from normal Balb/c foetal mice and assessed for PEDF expression by immunohistochemistry. Brown staining indicates areas of positive PEDF immunostaining. *Arrowheads: cranium*, chondrocytes; *digit*, chondrocytes; *intestine*, villus; *stomach*, mucosa; *kidney*, glomerulus; *lung*, alveolus; *spleen*, lymphoid precursor cells; *liver*, hematopoietic cells; *brain*, neuron; *back of eye*, retina; *lens*, white - lens fibre cells, black – lens epithelial cells; *skin*, follicle. *Scale bar* = 100 μm. (For interpretation of the references to colour in this figure legend, the reader is referred to the web version of this article.)

2.2. PEDF decreases cell cycling, causes apoptosis and activates caspase-2

PEDF dose-dependently reduced growth of human liposarcoma (Fig. 4a) and chondrosarcoma (Fig. 4b) cells, but did not have such an effect on 3 different colorectal cancer cell lines (Fig. 4c). Similar inhibition was noted in PC3 (Fig. 4d) and MDA-MB231 cells (Fig. 4e). PEDF decreased cell cycling in PC3 (Fig. 4f) and MDA-MB231 (Fig. 4g) cells, while increasing apoptosis in both cell lines (Fig. 4h and i). Electron microscopy confirmed apoptotic features in PEDF-treated cells (Fig. 4j and k). This was evidenced by membrane injury with the cell membrane experiencing blebbing and the nuclear membrane assuming an irregular shape. Chromatin condensation as well as evidence of nuclear fragmentation was noted, while in the cytoplasm, increased vacuolization was evident. When PC3 (Fig. 4l) and MDA-MB231 (Fig. 4m) cells were treated with PEDF, then injected orthotopically into tibiae of mice, tumor volumes were substantially lower ($p < 0.001$), demonstrating that in a bone environment, PEDF was highly active against both these osteotropic tumor cells' survival and growth. When a panel of cell cycle and apoptosis markers was assessed *via* immunoblotting, some interesting findings were observed (Fig. 4n). For PC3, there was a marked increase in p38, p63, E2F1 and Akt, while in MDA-MB231 cells, p63 and Chk1 were elevated, while E2F1 was reduced this time (Supplementary Fig. 1a). PEDF treatment did not cause a decrease in expression of any of the other markers for cell cycling, and these included NFκB, c-Jun, c-Fos, Chk1, Chk2, p-Akt, ERK1/2, p-ERK and JNK1. In regards to apoptosis markers, for PC3, there was increased presence of FasL and NOXA, with a reduction in Max and PPAR-γ (Supplementary Fig. 1b). For MDA-MB231, Fas and Max were increased, as was PPAR-γ this time. There was a downregulation of the c-*myc* oncogene. The most salient finding however was the consistency in activation of caspase-2 across both cancer cell types, and clear downregulation of its partners in PIDD, PKCδ and ICAD. Other apoptosis molecules such as Fas, Bcl-2 and Bax were unperturbed by PEDF treatment.

PEDF works together with zoledronic acid to control breast cancer growth in the murine bone, but inhibits tumor-mediated osteolysis better in the absence of zoledronic acid.

Current therapeutic approaches are largely two-fold: kill or control the tumor cells and preserve the bone quality, with recent research attempting to regenerate degraded bone. We provide evidence here that PEDF's action against metastasizing bone tumors are two-fold. Mice were administered PEDF + ZA over a period of 2 months. Firstly, mouse weights between treatments did not differ (Fig. 5a). Aggregate tumor volumes were the least in the combination (PEDF + ZA) cohort (Fig. 5b). When representative tumors were stained with $HgCl_2$ and scanned, the extra 'tissue' mass in the lower limb can be clearly seen, except in the combination treatment group where the limb has minimal tumor present (Fig. 5c). This is consistent with tumor measurements and volume derivations with a volume for the combination treatment group almost 50% of the untreated cohort (Fig. 5d). Of note is the fact that none of the tumors in the combination treatment group demonstrated necrosis and limb use was 100%, similar to PEDF treatment alone which is a promising finding (Fig. 5e). MicroCTs and X-rays revealed an almost intact tibial bone quality for the PEDF alone group (Fig. 5f and Supplementary Figs. 2 to 5), and this was corroborated with the highest level of tibial bone volume in the PEDF alone cohort; almost

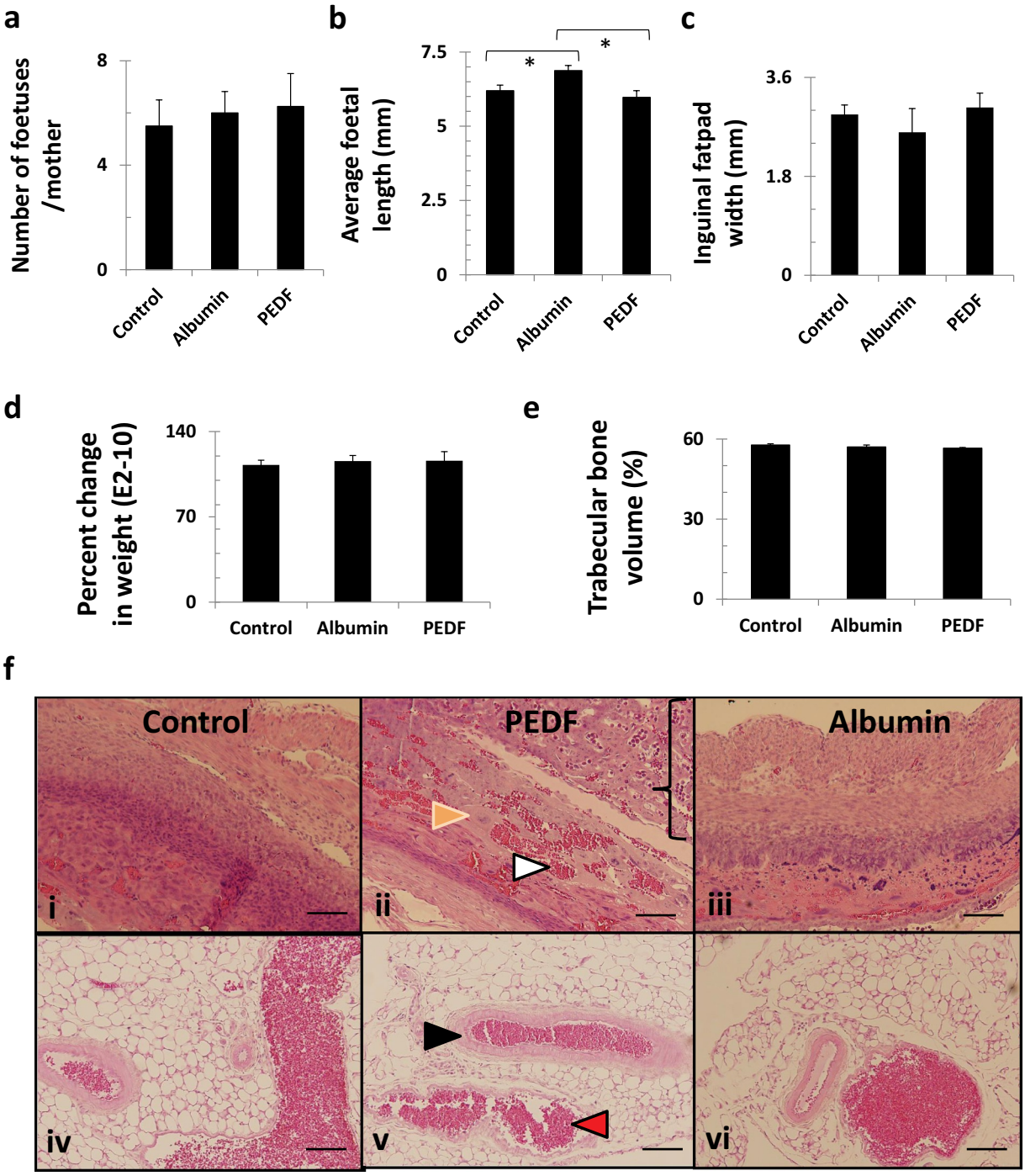

Fig. 2. Effect of PEDF on developing murine foetus.
(a) Average number of foetuses per pregnant mouse. (b) Average foetal length [crown (black arrowhead) to rump (yellow arrowhead)]. *$p < 0.05$. (c) Average relaxed inguinal fatpad width in pregnant mice. (d) Average percent change in weight in pregnant mice. (e) Average trabecular bone volume in femurs of pregnant mice. (f) Haematoxylin and eosin-stained paraffin sections showing foetal tissue (i-iii) and placental tissue (iv-vi). (g) Haematoxylin and eosin-stained paraffin sections showing pancreatic tissue (i-iii), inguinal adipose tissue (iv-vi) and skeletal muscle tissue (vii-ix). *Key to individual images (arrowheads)*: *white*, maternal blood lacuna; *orange*, giant trophoblast cell; *black*, vein; *red*, artery; *yellow*, islet of Langerhans; *blue*, septa; *green*, blood vessel in pancreatic parenchyma; *grey*, basophilic basal region of serous acinar cells; *pink*, acidophilic apical region of serous acinar cells. The circled areas show magnified sections containing acinar cells. *Black scale bar* = 400 μm, *yellow scale bar* = 40 μm. (For interpretation of the references to colour in this figure legend, the reader is referred to the web version of this article.)

50% higher than the untreated group (Fig. 5g). In fact, while bone volume could not be undertaken for the fibulae due to the extensive level of damage especially in the control group, once again PEDF provided the greatest level of protection against cancer cell-mediated degradation. EPMA analysis focussing on the PEDF alone treatment confirmed that the tibiae were well-preserved in this group (Fig. 5h).

3. Discussion

PEDF was ubiquitously present in all foetal tissues that were examined, particularly in the cranial and digital sections, within the chondrocytes. It is interesting to note that it is prominently expressed in a variety of foetal tissues, perhaps not surprising given its role in stem

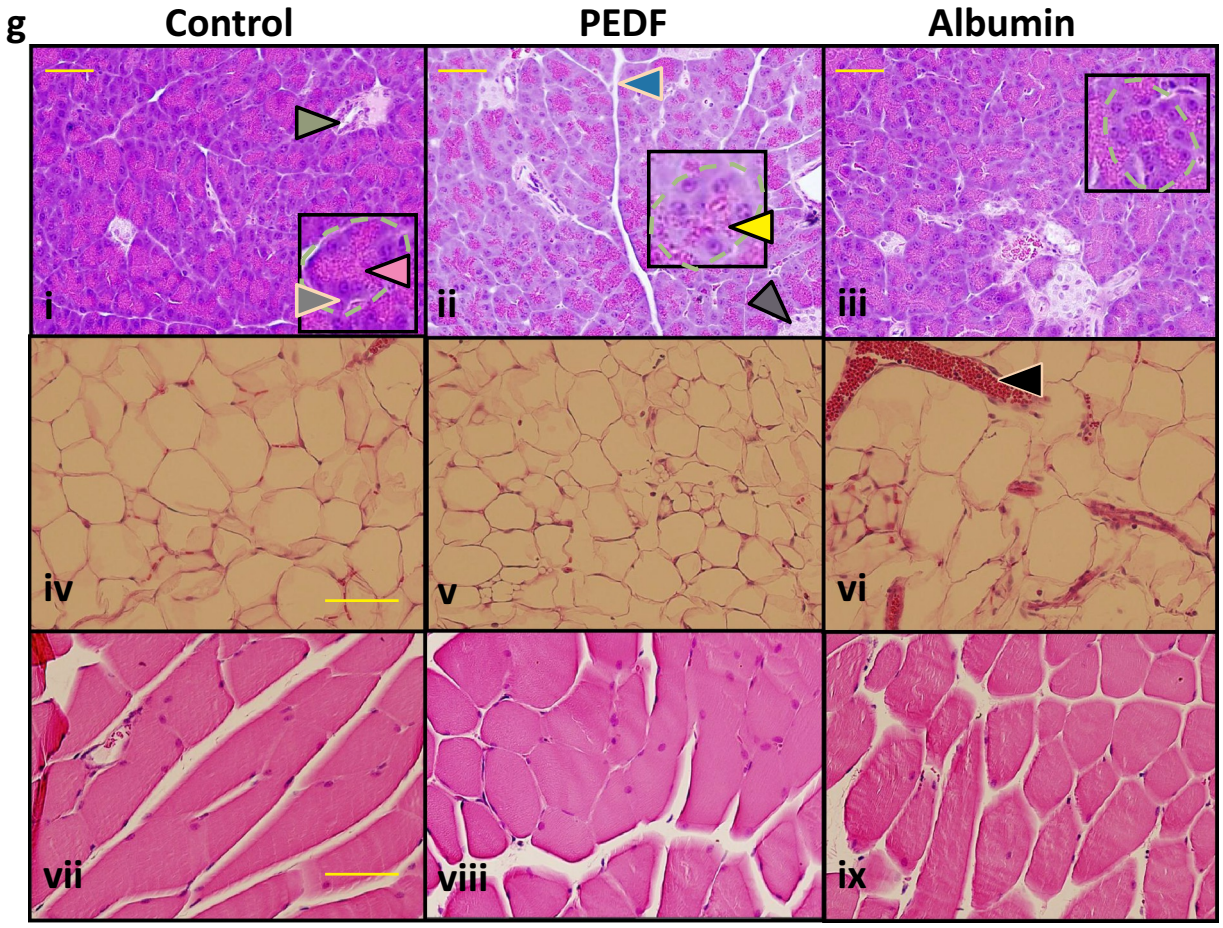

Fig. 2. (*continued*)

cell support [7,8,38,39]. Nearly two decades ago [40], PEDF was demonstrated to be more potent than endostatin and angiostatin in curbing development of new blood vessels in the CAM assay. Thus, if PEDF is to be used therapeutically in future, against cancer or other diseases, it is both prudent and imperative that it is tested for any adverse effects on physiological angiogenesis. In keeping with this, we chose a model that has angiogenesis at its core, namely, foetal development. In summary, PEDF was found to not perturb foetal development when administered continuously. Blood supply mostly *via* lacunae in the space between maternal and foetal vasculatures were normal in the PEDF cohort. Furthermore, it is known that during pregnancy, bone tissue turns over much more rapidly, with maternal calcium being mobilized during late pregnancy as a result of the sheer demand for calcium by the foetus on maternal calcium repositories, the main one being bone [33]. Thus, if PEDF has an untoward effect on bone turnover, we would be able to detect it with microCT, but this was not the case as assessed on maternal trabeculae bone volume. Additionally, histology revealed that developing foetal bone was also unperturbed by PEDF. However, we emphasise that gross analysis of the fetal mouse found no adverse effects of PEDF administration on fetal weight gain and growth during the first two-thirds of fetal life, and further intricate analysis on individual organs and tissues under development will no doubt shed more definitive light on safety of PEDF *in utero*.

The only impact we could see was that on pancreatic tissues of pregnant mice, where there was a discernible decrease in the quantity of zymogen granules present in the secretory acini. The function of the acinar cell is largely synthesis of enzymes and zymogens in the pancreatic juice to aid breaking down complex molecules in the gut to assist in digestion [41]. The cells are characterized by large quantities of rough endoplasmic reticulum and granules that have budded off the Golgi apparatus and collected at the apical pole of the cell destined for secretion. These granules are stored until the cell receives a trigger to degranulate and expel their contents into the lumen of the acinus. Thus, PEDF may either reduce production of such granules, or alternatively, stimulate their expulsion. A clearly visible widening of the intercalated ducts between the acini would support the latter hypothesis. This would add another level of function for PEDF in its regulation of metabolism, this time at the point where food is broken down in the gut. This remains to be tested. In regards to metabolism, PEDF's existing roles include induction of insulin resistance in skeletal myocytes [42], insulin secretion from pancreatic β-cells [43], hepatic insulin signalling [44], enhancement of glycolysis in skeletal myocytes [45], and lipid metabolism in cardiomyocytes [46]. Thus, PEDF is increasingly being implicated in various levels of metabolism.

Previously, we have shown that PEDF is efficacious against OS [32]. In the current study, a more aggressive human OS cell line, 143B, was employed to see if PEDF maintains its efficacy in a more devastating state of the disease [47]. We know that aggressive OS traverses the growth plate cartilage, an area where PEDF is prominent in bone [48], which is why we sought to test PEDF against a more aggressive OS cell line. In addition, we added Dox therapy to PEDF to see if any synergism is noted. Interestingly, PEDF emerged as more efficacious than Dox. Dox is a standard drug used against OS clinically, though it suffers from severe cases of cardiotoxicity [35,36] amongst other side-effects [49]. In this study, we demonstrated that not only is PEDF efficacious *per se*, but it protects the heart tissue from damage induced by Dox. Furthermore, PEDF showed chemoprotective effects in not only the heart, but the small intestine and the testis in the current study. Such chemoprotective abilities of PEDF add yet another dimension to its efficacious nature.

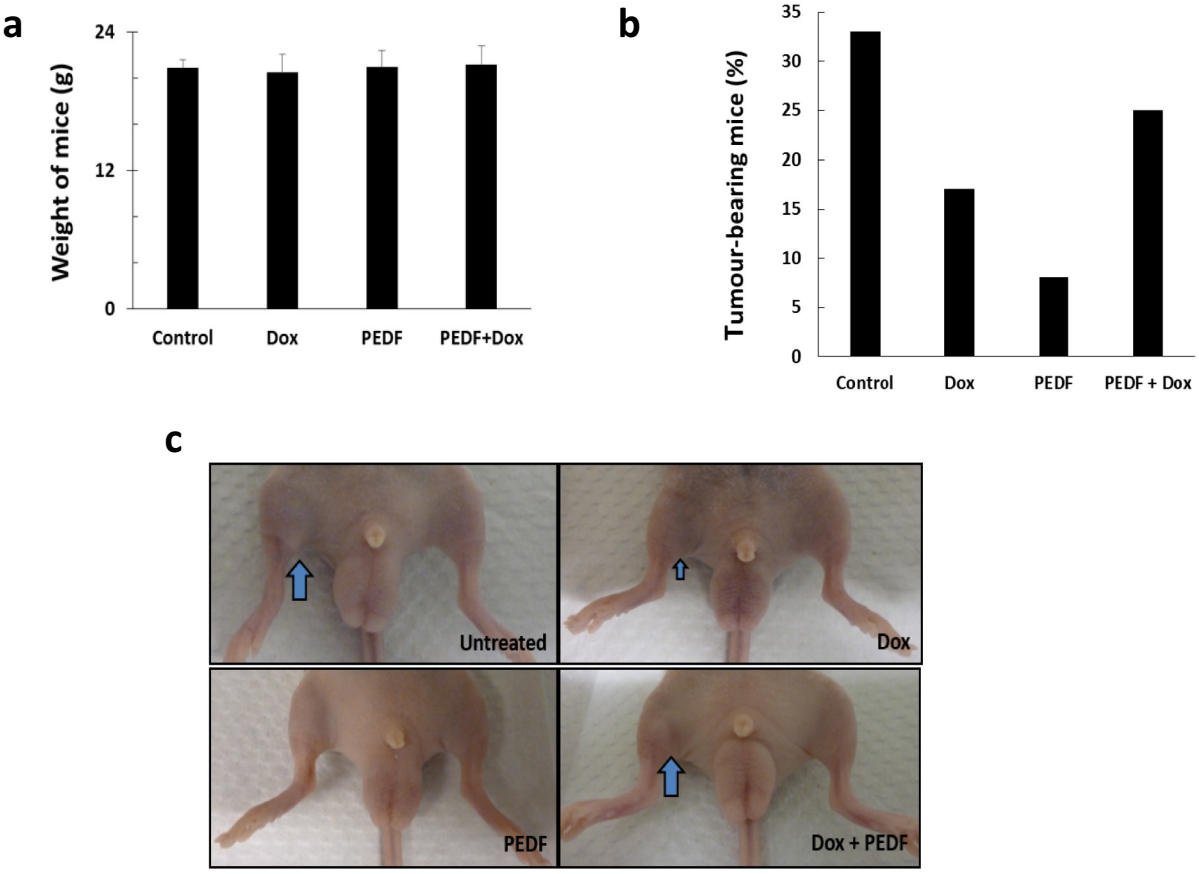

Fig. 3. PEDF synergizes with doxorubicin (Dox) against osteosarcoma while acting as a chemoprotectant.
(a) No changes in animal weights in mice administered any of the treatments compared to control (untreated). (b) Percentage of 143B tumor-bearing mice was the least in the PEDF cohort. (c) Representative photos of animals from each cohort. (d) H & E-stained sections of representative tumors from each group. *Scale bar* = 200 μm. (e) Cardiac tissue H&E sections, showing cellular vacuolation (*arrowheads*) in the Dox-treated group. *Scale bar* = 100 μm. (f) Graph of cellular vacuolation. (g) H&E sections showing that the number of hyperplastic spots in the small intestine increases in the Dox group. *Scale bar* = 100 μm. (h) Graph of increased hyperplastic spots in the small intestine, which is reduced by PEDF. *Scale bar* = 50 μm. (i) H&E staining showing changes in the seminiferous tubules by Dox. (j) Graph of percent normal seminiferous tubules showing reduction by Dox, and protection by PEDF. (k) H&E staining of skin sections showing loss of hair in the Dox group, with some follicle growth in the PEDF + Dox group. *Scale bar* = 50 μm. (l) H&E staining of white adipose tissue from the inguinal fatpad region. *Scale bar* = 50 μm.

Apart from OS, PEDF dose-dependently reduced growth of human liposarcoma and chondrosarcoma cells, but did not have such an effect on different colorectal cell lines. Thus, its anticancer effect is particular effective against sarcomas, that is, those arising from MSCs. A significant level of inhibition was noted in human prostate and human breast cancer cells, carcinoma cells that harbor a strong tendency to metastasize to bone. Akin to our previous findings with OS [10,22] and chondrosarcoma [18] cells, PEDF decreased cell cycling in prostate and breast cancer cells, while increasing apoptosis in both. When either prostate or breast cancer cells were treated with PEDF, then injected orthotopically into tibiae of mice, tumors volumes were substantially lower in the PEDF cohort. Thus, PEDF seems to have potent activity against tumor cells either arising from or taking residence post-metastasis in bone. PEDF treatment of both human prostate and breast cancer cells consistently activated caspase-2. Interestingly, while caspase-2 was activated, its partners in apoptosis execution, namely PIDD [50], PKCδ [51] and ICAD [52] were all downregulated, suggesting that apoptosis *via* caspase-2 was not likely despite activation of this caspase. While this phenomenon deserves further study, it is known that caspase-2 is activated during osteoblastic differentiation induced by bone morphogenetic protein-4, BMP-4 [53]. Other apoptosis molecules such as Fas, Bcl-2 and Bax were unperturbed by PEDF treatment.

We provide seminal evidence here that PEDF's action against metastasizing bone tumors are two-fold. It preserves the bone from greater destruction by the imposing tumor growth. This is not that surprising given that PEDF has been shown to induce osteogenic activity at the bone [11] and even in muscle tissue [54]. In the current study, it was noted that PEDF can act together with an anti-osteoclast agent such as ZA to control secondary tumor growth in bone. It is of interest that when combined with ZA, PEDF is unable to preserve bone volume as well as when it is administered alone. A plausible hypothesis for this is that despite its anti-osteoclastogenic role [21], PEDF perhaps needs the activity of osteoclasts in bone preservation when bone is being destroyed by tumor growth. This warrants further investigation. In this case, preservation would incorporate *de novo* bone formation as tumor destruction is still expected when PEDF is administered alone. This is also attested to by the fact that all limbs were functional in the PEDF cohort, similar to the case in the combination treatment cohort.

4. Conclusion

PEDF is ubiquitous in murine embryonic tissues, and continuous administration to pregnant mice does not adversely affect foetal health, ruling out any untoward effects against physiological angiogenesis and foetal development. In the case of the devastating childhood bone cancer osteosarcoma, not only does PEDF have direct anticancer activity *per se*, but it protects against the toxicity of a commonly used frontline chemotherapeutic, doxorubicin, in the heart, small intestine

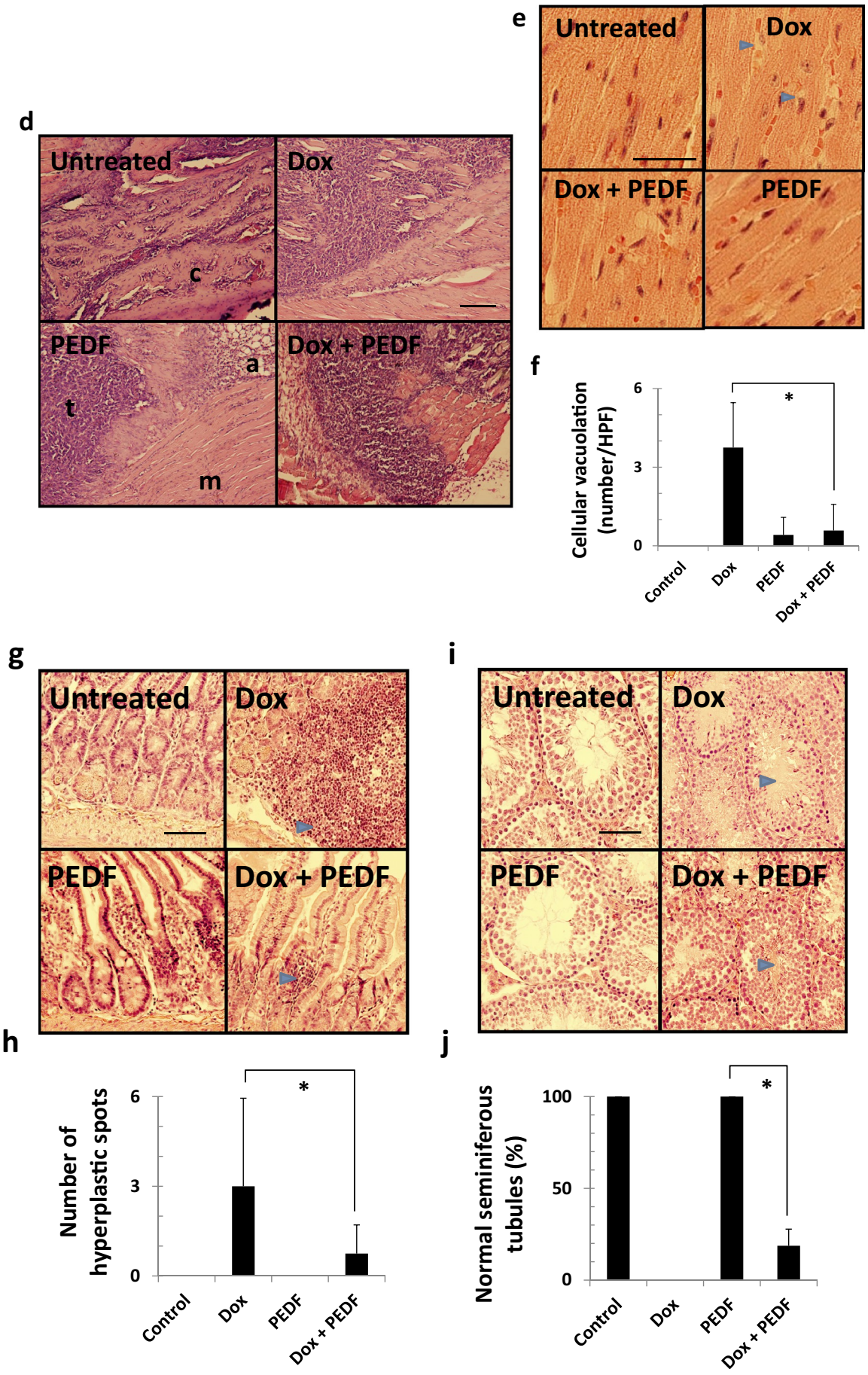

Fig. 3. (*continued*)

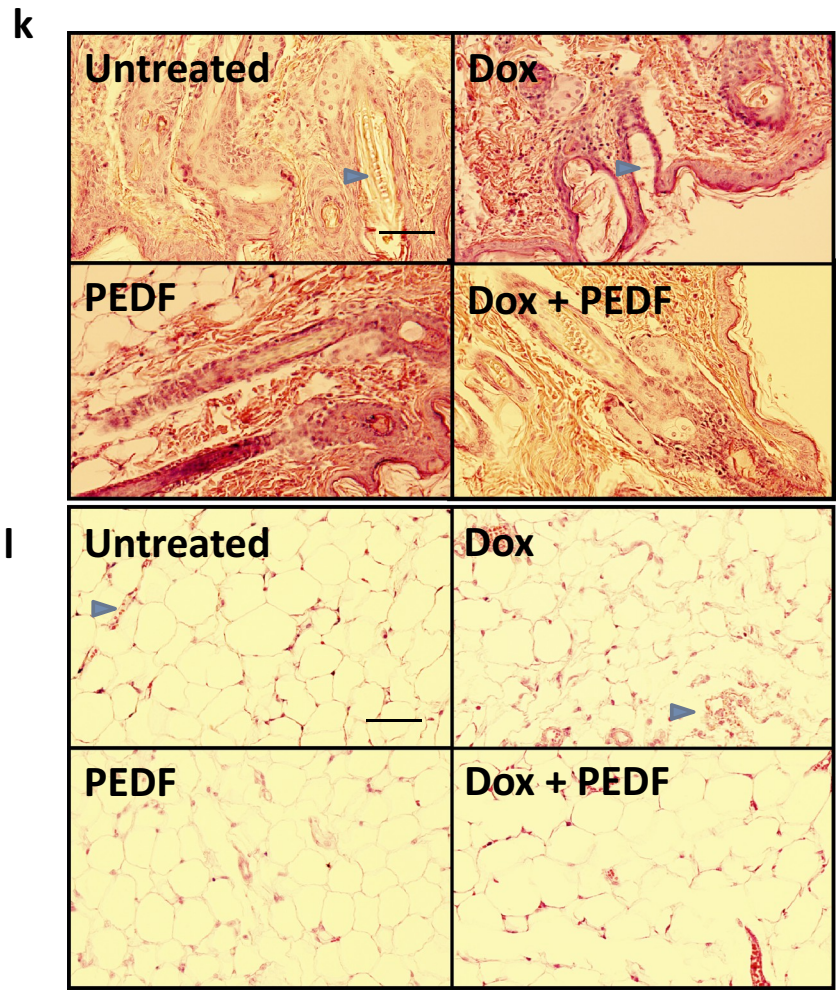

Fig. 3. (*continued*)

and testes. In orthotopic models of prostate and breast cancers in bone, PEDF significantly reduced tumor volumes. When combined with the frontline anti-osteoclast chemotherapeutic, zoledronic acid, continuously-administered PEDF significantly reduced breast tumor volume at the bone, and was able to preserve the quality of bone better than the combination therapy. PEDF thus has beneficial effects against bone tumors as it can directly inhibit tumor growth and progression plus preserve the quality of bone at the lesion site, while not having untoward effects against physiological angiogenesis, but able to serve as a chemoprotectant, making it an ideal candidate for possible future clinical testing.

5. Materials and methods

5.1. Materials

Recombinant PEDF was purchased from MD Bioproducts (Bethesda, MD, USA). ECL Prime immunoblotting detection reagent kit was purchased from GE Healthcare Amersham (Melbourne, VIC, Australia). Dox and penicillin/streptomycin were purchased from Sigma-Aldrich (St Louis, MO, USA, Australia). Cell-Titer (CT) Blue cell viability assay and Apo-ONE Homogeneous Caspase-3/7 Assay were purchased from Promega (Madison, WI, USA). Image-iTTM LIVE Green Reactive Oxygen Species Detection Kit (I36007) was obtained from Molecular Probes (Melbourne, VIC, Australia). Adenosine triphosphate (ATP) Colorimetric/Fluorometric Assay Kit was purchased from BioVision (Milpitas, CA, USA). All other reagents were obtained from Sigma-Aldrich unless otherwise stated.

5.2. Cell lines and media

Human osteosarcoma cell line 143B, human breast cancer cell line MDA-MB231, human prostate cancer cell line PC3, murine H9c2 cell line, murine C2C12 myoblasts, human colorectal cancer cell line HT29, human colorectal cancer cell line DLD-1, human colorectal cancer cell line RKO and rat cardiomyocyte H9c2 cells were obtained from the American Tissue Culture Collection, ATCC (Manassas, VA, USA). The human chondrosarcoma cell line JJ012 was kindly provided by Dr. J. A. Block (Rush University Medical Centre, Chicago, IL, USA). Human skeletal muscle myoblasts (HSMMs) were purchased from Lonza (Walkersville, MD, USA) and were used within 5 passages from receipt. SW872 was obtained from Dr. David Thomas (Peter MacCallum Cancer Centre, Melbourne, VIC, Australia) and used within 10 passages. Cells were cultured in Dulbecco's Modified Eagle Medium (DMEM) or Roswell Park Memorial Institute medium (RPMI) supplemented with 10% foetal bovine serum (FBS) and 1% antibiotics and antimycotics at 37 °C within a humidified 5% CO_2 chamber. Media and supplements were from Sigma-Aldrich.

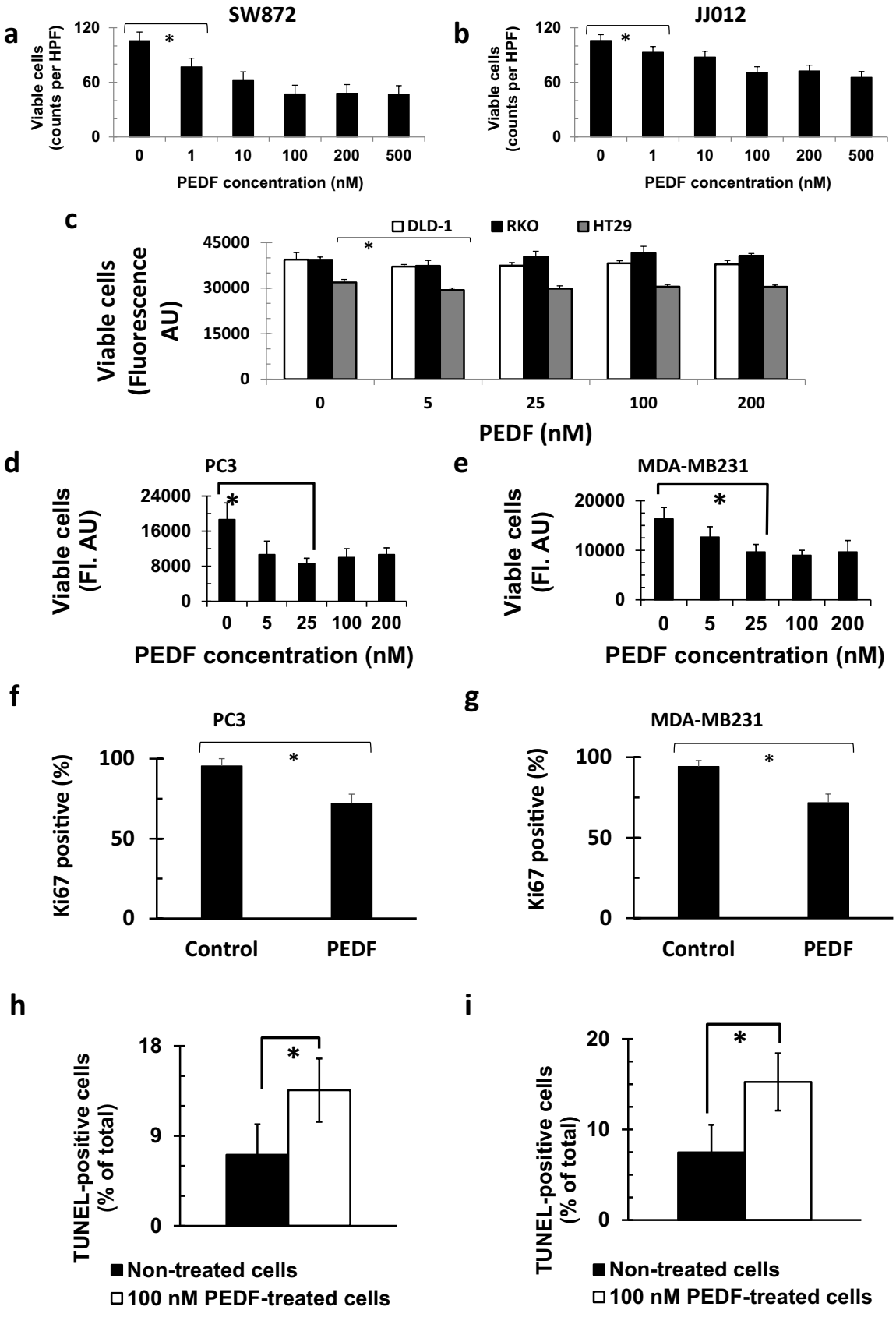

(caption on next page)

Fig. 4. PEDF reduces cell cycling and increases apoptosis in human prostate and breast cancer cell lines.
Dose-dependent changes in human tumor cell growth in (a) liposarcoma, (b) chondrosarcoma, (c) colorectal carcinoma (3 lines), (d) prostate and (e) breast cancer cell lines. PEDF (100 nM) decreases cell cycling (f,g) and increases apoptosis (h,i) in a human prostate and breast cancer cell line respectively. Chromatin condensation (blue arrowhead) and cell membrane blebbing (yellow arrowhead) in human (j) prostate and (k) breast cancer cell lines. PEDF reduces growth of tumor in orthotopic models of (l) prostate and (m) breast cancer growth in bone. * $p < 0.1$, $n = 5$. (n) Immunoblotting analysis of various tumor-related cell cycle and apoptosis markers in prostate and breast cancer cells showing p63 consistently elevated in both cell lines by PEDF (100 nM), and an increase caspase-2 activation but decrease in caspase-2-related markers (PIDD, PKC-δ, ICAD) by PEDF (100 nM). (For interpretation of the references to colour in this figure legend, the reader is referred to the web version of this article.)

5.3. PEDF expression in foetal mice

While it is known to be expressed in a few adult tissues such as bone [48] and skin [55], PEDF's distribution in the body is largely unknown. Prior approval for this study was obtained from the St Vincent's Health Animal Ethics Committee. Animal care was in accordance with institution guidelines and monitored by the resident Animal Welfare Officer. Mice were fed and hydrated *ad libitum*. Balb/c pregnant mice at E10 were euthanized before foetuses were fixed in 10% buffered formalin, processed histologically, and stained with haematoxylin and eosin (H&E). Foetal sections were analysed *via* immunohistochemistry for PEDF expression using the procedure outlined under 'Immunohistochemistry'.

5.4. In utero testing

Approval was obtained from the Curtin University AEC committee prior to experimentation. Animal care was in accordance with institution guidelines and monitored by the resident Animal Welfare Officer. The gestation period E5–E10 was chosen as it represents rapid development in the foetuses, enabling any effects against angiogenesis to be detected. Mice were fed and hydrated *ad libitum*. Pregnant Balb/c mice at E10 were subcutaneously implanted [56,57] in quadruplicate with model 1002 osmotic pumps (Durect Corp, Cupertino, CA, USA) filled with PEDF or albumin (Sigma-Aldrich) to deliver at a rate of 50 μg/kg/day. Pumps filled with water served as vehicle controls. Mice were checked every day to monitor health, surgical site, and for any signs of complication with pregnancy (example bleeding from the reproductive tract). At E15, mice were euthanized, weighed, the number of foetuses counted, foetuses measured from crown to tail bone, and resting inguinal fatpad width (unstretched) measured with digital callipers. Foetuses, placenta and inguinal fatpad were harvested and processed histologically. Hindlimbs of pregnant mice were scanned with microCT and images analysed (CT-Analyser, Bruker, Kontich, Belgium).

5.5. Viability assay

The proliferation of cells following PEDF treatment was assessed using the Cell Titer Blue assay fluorimetrically according to the manufacturer's instructions using a multimode Enspire 2300 Plate Reader (Perkin Elmer, Akron, OH, USA) as before [58]. All treatments including controls were performed in quadruplicate. Results were averaged, standard deviations calculated and presented as either cell counts per high power field (HPF; 200× magnification) or fluorescence units.

5.6. Caspase-3/7 apoptotic assay

Cells were treated as before. The activation of caspase 3/7 was monitored with an ATP assay kit as per manufacturer's instructions. Briefly, 100 μL of Apo-ONE Caspase-3/7 reagent was added into each well including controls. The plate was gently swirled to mix the contents of the wells and was left incubating for 1 h. The samples were analysed with an Enspire microplate reader at an Ex/Em of 492/524 nm. The samples were observed again at day 3. All treatments including controls were performed in quadruplicate.

5.7. PEDF plus doxorubicin efficacy against orthotopic murine osteosarcoma model

Animal experimentation was prior approved by the Curtin University Animal Ethics Committee. Animal care was in accordance with institution guidelines and monitored by the resident Animal Welfare Officer. Five-week-old Balb/c nude male mice were purchased from the Animal Resource Centre, Perth, Australia. Mice were fed and hydrated *ad libitum*. The mice were anaesthetized with inhalation isoflurane. 1×10^6 cells/mL of 143B osteosarcoma cells were suspended in 50% Matrigel (BD Biosciences, Melbourne, VIC, Australia) and 20 μL of the 143B/Matrigel mixture was injected into the right tibia of the mice with disposable 26G needles [47,59]. The mice were closely monitored after injection until fully recovered and were left for a week to allow tumor growth before commencement of a 4-week-long Dox and PEDF administration. The mice were checked daily for food intake and signs of distress every 3 days for weight changes.

Forty-eight mice were injected with 143B tumor cells (12 mice per group × 4 treatment groups). The 4 treatment groups include *(a)* distilled water as negative control, (*b*) 1 mg/kg Dox, (*c*) 50 μg/kg PEDF and (*d*) 50 μg/kg PEDF + 1 mg/kg Dox. All drugs and water were injected intraperitoneally every 3 days. At the end of 4-week-drug administration, all mice were euthanized by isoflurane inhalation, followed by cervical dislocation. Tumors were measured in the anteroposterior (AP) and lateral (L) planes with callipers. Tumor volumes were calculated using the formula [60,61]: 4p/3 [0.25 (AP × L)] [2] as was the percentage of tumor-bearing mice. Tumor-bearing limbs were harvested along with skin, adipose tissue (inguinal fatpad), intestines, testes and hearts. All specimens were fixed in 4% paraformaldehyde and the limbs were decalcified in hydrochloride. Sections (5 μm) were prepared and stained with H&E prior to light microscopy under an upright Olympus IX53 (Olympus, Melbourne, VIC, Australia) microscope.

5.8. Cell cycling analysis

To assess whether cells were cycling, immunocytochemistry for the marker Ki67 was performed as before [18]. In brief, 4% paraformaldehyde-fixed cells were permeabilized with 0.2% saponin and 0.5% bovine serum albumin (BSA), and blocked with 2% normal serum (Dako, Melbourne, VIC, Australia) for 30 min. Cells were then incubated overnight with primary Ki67 antibody (Santa Cruz Biotechnology, Santa Cruz, CA, USA), at a 1:250 dilution), after which cells were treated with secondary biotinylated antibody (Dako) at a 1:2000 dilution for 30 min. Slides were treated with streptavidin linker and signal amplifier (Vectastain, Vector Labs, CA, USA), prior to staining with diaminobenzidine (DAB). Cells were rinsed with water, mounted in 75% glycerol, coverslipped and imaged using a Nikon eclipse Ti inverted microscope (Nikon, Melbourne, Australia) and SPOT Advanced software (SciTech, Melbourne, VIC, Australia).

5.9. Terminal deoxynucleotidyl transferase (TdT) dUTP nick end labelling (TUNEL) assay

The TUNEL assay (Promega, Melbourne, Australia) was performed as before [56]. Briefly, cells were fixed in 4% paraformaldehyde,

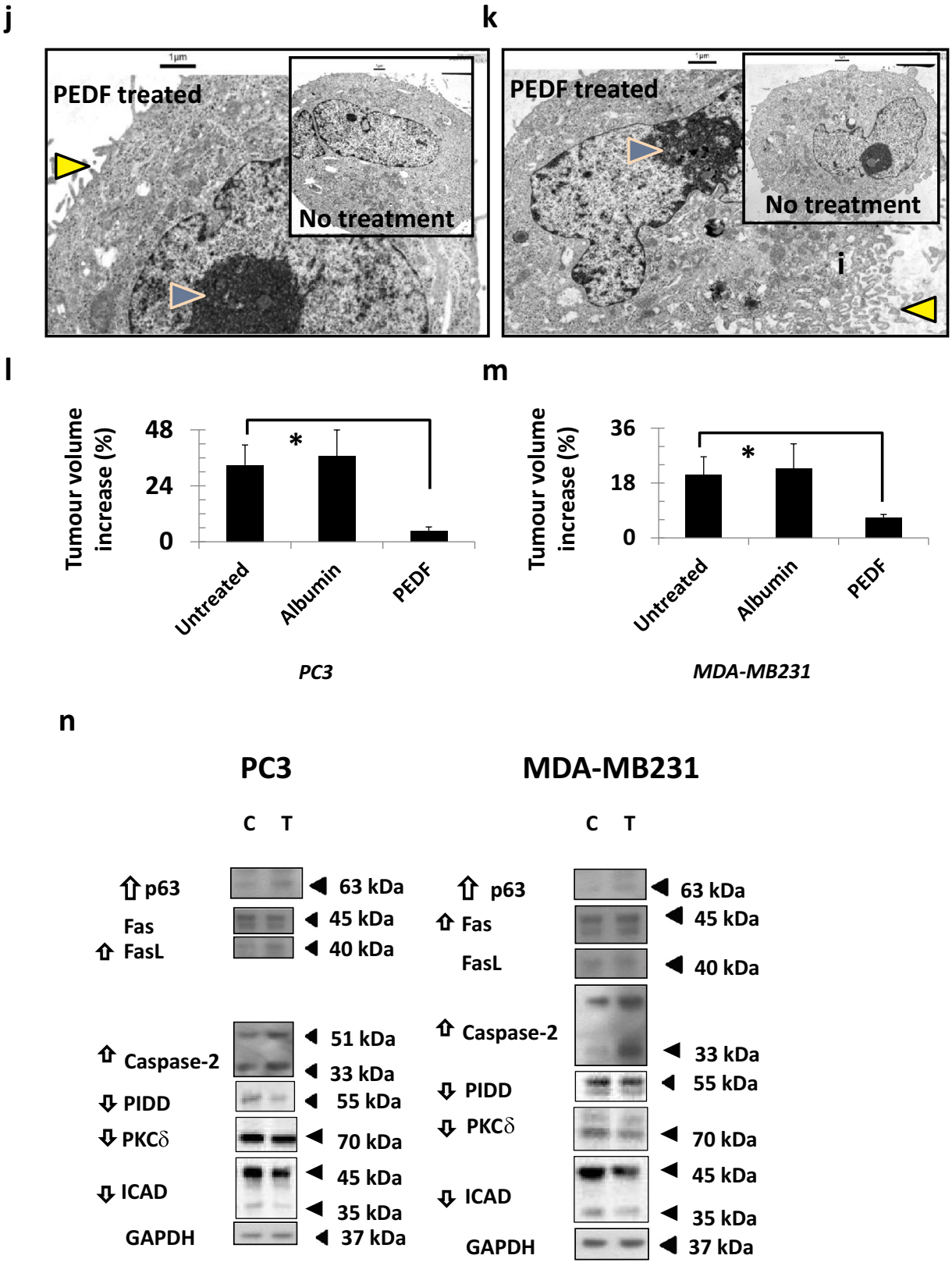

Fig. 4. (*continued*)

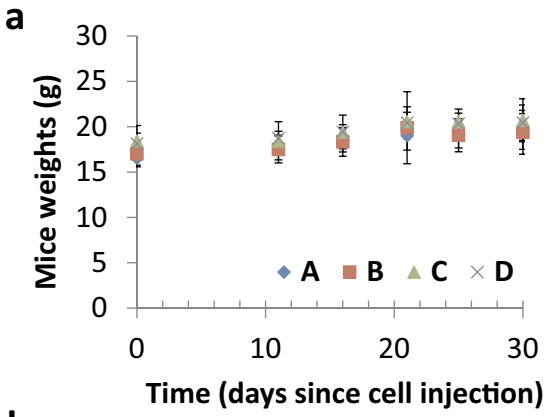

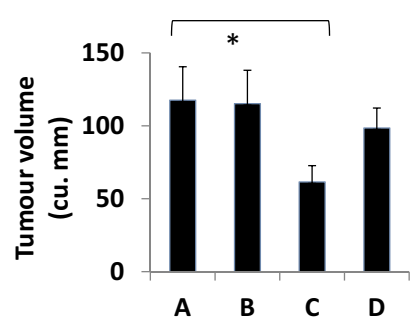

e

Group	Untreated (A)	ZA (B)	ZA + PEDF (C)	PEDF (D)
Limb use (%)	70	60	100	100
Necrosis (%)	30	40	0	10

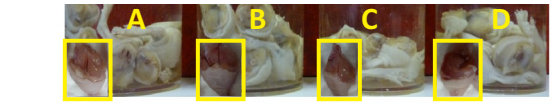

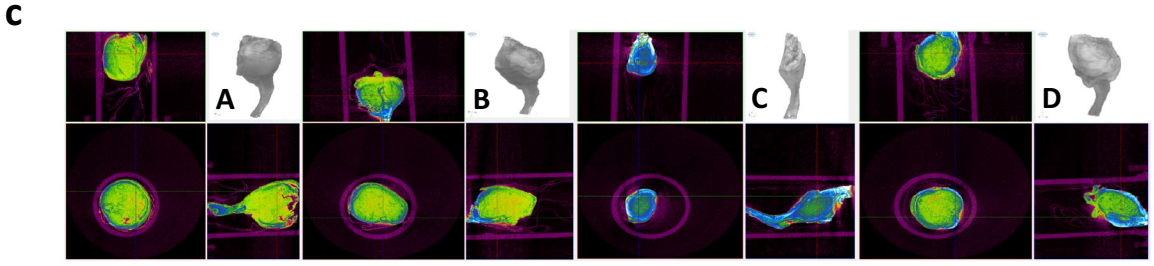

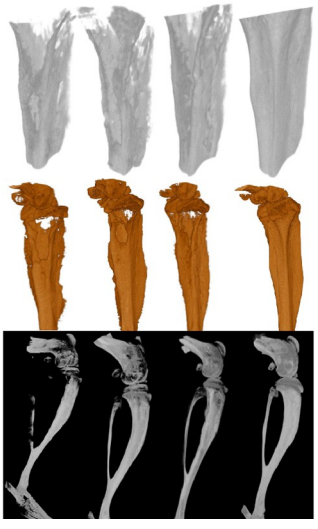

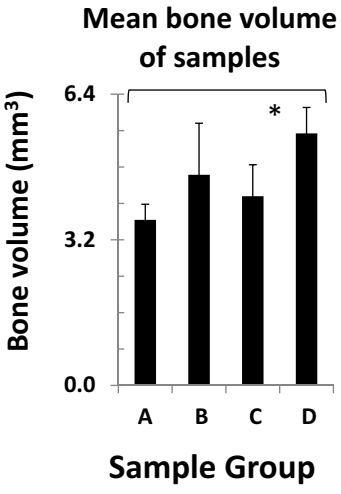

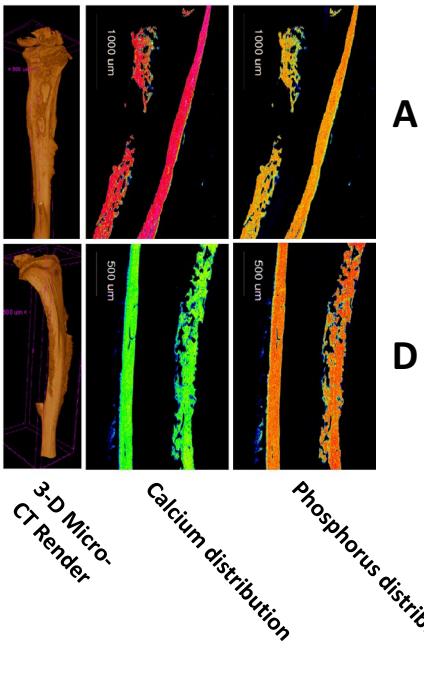

(caption on next page)

Fig. 5. PEDF combined with zoledronic acid reduces tumor growth and PEDF alone preserves bone volume.
(a) Weights of mice bearing orthotopic OS tumors. (b) Collection of all tumors showing the extent of tumor growth at the tibia. (Insert) lateral close-ups of representative tumors. (c) Limbs from each group were stained with $HgCl_2$ for soft tissue contrast and imaged with conventional micro-CT (19 μm resolution). Software used was SkyScan-bundled Data Viewer, "Colour 1" view (greyscale tissue densities represented in different colours using a preset thresholding range). (d) Tumor volumes across treatment groups. (e) Percentage limb use and necrosis in individual groups. (f) Micro-CT and X-ray images of legs from treatment groups A–D, left-to-right. (g) Extent of bone volume across treatment groups. Note that group D treatment has increased bone volume by 56% compared to group A ($p < 0.01$). (h) EPMA images of representative murine tibia of group A *versus* group D.

followed by permeabilization in 0.2% Triton X-100. Cells were equilibrated before labelling with recombinant terminal deoxynucleotidyl transferase enzyme. Horseradish peroxidase-labelled streptavidin was bound to biotinylated nucleotides and detected using peroxidise substrate, hydrogen peroxide, and DAB. Apoptotic cells visualized under a light microscope were stained dark brown. Cells were imaged with a Nikon Eclipse TE2000-U microscope (Nikon, Melbourne, VIC, Australia) and photographed with SPOT Advanced software.

5.10. Electron microscopy

For cell morphological analysis, transmission electron microscopy (TEM) was performed on PC-3 and MDA-MB231 cells treated ± 100 nM PEDF for 24 h prior to fixation with 2.5% glutaraldehyde/0.1 M cacodylate buffer (pH 7.4) for 1 h [62]. Cells were post-fixed with 2.0% osmium tetroxide/deionized water for 1 h before dehydration in a gradient of acetone, followed by infiltration with Spurr's resin and sectioning on an UltraCut-S microtome. In addition, sections were stained with uranyl acetate/lead citrate solution and imaged. TEM was performed on a Siemens 102 transmission instrument at 60 kV (Melbourne, VIC, Australia) in a blinded fashion.

5.11. Immunoblotting

Immunoblotting was performed on lysates from human tumor cells treated ± 100 nM PEDF by extracting cellular proteins using ice-cold RIPA lysis buffer (20 mM Tris-HCl, 150 mM NaCl, 1 mM EDTA, 1 mM EGTA, 1% NP40, 2.5 mM pyrophosphate, 1 mM β-glycerophosphate, 1 mM sodium vanadate) containing complete protease inhibitors (Sigma-Aldrich) [63]. Lysates were electrophoresed through a 4–20% gradient NuPAGE gel (Invitrogen, Melbourne, Australia) and electrotransferred to a polyvinylidene difluoride (PVDF; Invitrogen, Melbourne, VIC, Australia) membrane. Antibodies (cdc42, Rac1, uPA, uPAR, MT1-MMP, caspase-2, glyceraldehyde-3-phosphate dehydrogenase (GAPDH) and α-tubulin; Santa Cruz Biotechnology) were applied overnight at 4 °C, then secondary biotinylated antibodies (Dako) applied for 1 h at room temperature. Cleaved caspase-3 primary antibody was from Cell Signalling (Sydney, NSW, Australia). Antibodies were visualized with ECL Prime chemiluminescent reagent (GE Healthcare Amersham, Melbourne, VIC, Australia), and images acquired with a Gel-Doc EZ instrument (Biorad, Gladesville, NSW, Australia).

5.12. Immunohistochemistry

Tissue sections were deparaffinized with 100% xylene and rehydrated with various concentrations of ethanol [64,65]. Antigen retrieval was achieved with incubation of sections in 10 mM Tris and 1 mM EDTA (pH 9.0) for 12 min at high heat (~90 °C). Endogenous peroxidase activity was blocked with 3% hydrogen peroxide in phosphate buffered saline (pH 7.4). Blocking was achieved with bovine serum albumin (BSA), and tissues were subsequently incubated overnight at 4 °C with primary monoclonal antibody (Santa Cruz Biotechnology) for PEDF, MT1-MMP, HSP47, collagen I and MMP-2. Sections were then incubated overnight with secondary antibody (Dako). Tissue sections were treated with biotinylated link (Dako), followed by streptavidin-HRP (Dako). Staining was achieved with DAB. Counterstaining was subsequently achieved with haematoxylin and briefly with Scott's tap water (Sigma-Aldrich). Tissues were dehydrated in a series of ethanol washes in increasing concentrations (30, 70 and 100%) before a xylene rinse. Mounting was achieved with Depex solution (Sigma-Aldrich).

5.13. Breast and prostate cancer-in-bone model

Approval was obtained from the Curtin University AEC committee prior to experimentation. Animal care was in accordance with institution guidelines and monitored by the resident Animal Welfare Officer. Mice were fed and hydrated *ad libitum*. Intratibial injection [66] was chosen for osteotropic cancer-in-bone model as this provides a more controlled and reproducible growth of tumor in bone, mimicking the latter stages of the process of metastasis where cells establish in the bone. PEDF or BSA (100 nM) was mixed with 5×10^6 MDA-MB231 or PC3 tumor cells in 50% matrigel before orthotopic injection in a volume of 20 μL in the proximal tibia of five week-old Balb/c nu/nu mice using a 26G needle. Mice were monitored twice weekly prior to tumor development, and then three times weekly when tumors were palpable. At the end of the study (day 35), tumors were measured AP and longitudinally (L) with digital callipers. Taking tumor bulge into consideration, AP was measured left-to-right across the knee-cap and L was an anterior-to-posterior measurement of the tibia. Tibial tumor volume was calculated using the formula: 4p/3 [0.25 (AP × L)] [2], and tibial volumes subtracted using measurements from the non-tumor-bearing limb [67].

5.14. Zoledronic acid plus PEDF study

The *in vivo* procedures for this study were prior approved by the Curtin University Animal Ethics Committee. Animal care was in accordance with institution guidelines and monitored by the resident Animal Welfare Officer. Mice were fed and hydrated *ad libitum*. Balb/c *nu/nu* mice (male, 5 weeks old) were anaesthetized with isoflurane for 5–10 min of anaesthesia for cell injection and 20 min for the osmotic pump implantation. Mice were also administered a subcutaneous dose of two analgesics: meloxicam at 1.5 mg/kg and buprenorphine at 0.075 mg/kg. The buprenorphine was administered 30 mins prior to the procedure. This allows for minimizing the pain pathways being elicited and thus reduces overall pain. The meloxicam was administered upon mouse waking. Post-anaesthesia, cells were injected peri-tibial *via* 26G needles in a volume of 20 μL of matrigel-suspended 1×10^6 human breast (MDA-MB231) cancer cells as we have done before [34]. Animals were monitored closely after injection until fully recovered.

Mice were left to grow tumors for two weeks, and then 4-week-long osmotic pumps containing PEDF (50 μg/kg/d) or control solution were implanted subcutaneously [68]. At this point onwards, ZA was subcutaneously administered to mice at a dose of 120 mg/kg twice weekly, a dose we had used before [67]. Treatments ($n = 10$/group) involved (*a*) cells only (negative control), (*b*) cells + 50 μg/kg PEDF, (*c*) cells + 120 μg/kg ZA, and (*d*) cells + 50 μ/kg PEDF + 120 μg/kg ZA. For the combination group of PEDF + ZA, mice were monitored twice daily for the first 3 times of combined treatment to check whether mice were feeling any discomfort, even though none was anticipated as both agents are relatively safe within this timeframe of analysis and doses proposed.

After injection, animals were permitted unrestricted movement within their cages. Mice were kept for a further 8 weeks in cages with appropriate food and water. They were monitored daily, and every second day, mice were weighed and tumors measured along 2 dimensions (AP, anterioposterior length, and L, mediolateral length) on the hindlimb once tumors reached a palpable size. Tumor volumes were calculated using the formula: 4p/3 [0.25 (AP × L)] [2]. At the end of study, mice were euthanized, and tumor-containing hindlimbs were harvested, imaged *ex vivo* with microCT, then processed for undecalcified electron probe microanalysis (EPMA) to locate the calcium and phosphate labels in bone, and subsequent decalcified histology was performed at the bone-tumor interface.

5.15. MicroCT

Mice tibiae were dissected free of soft tissue and placed in the bed of a Skyscan 1076 *In Vivo* X-ray microtomograph [54]. Two-dimensional projections were obtained using an X-ray source setting of 70 kV and 139 mA, with beam filtration through a 0.5 mm aluminium filter. Three scan projections were averaged per step, through the 180° of rotation at 0.5° step increments with exposure times of 1070 ms. The two-dimensional raw image projections were reconstructed using a modified Feldkamp back-projection algorithm, with the cross-section to image conversion values set to 0.0–0.0367 for all samples, using bundled vendor software (NRecon, version 1.6.9, Skyscan NV, Belgium). The resulting reconstructed transverse image slices were analysed using vendor-supplied analysis software (CTAnalyser, Bruker, Kontich, Belgium), with semi-automated contouring. The selected region of interest spanned approximately 100 × 18 μm slices, and was analysed using morphometric software to determine bone volume.

5.16. Electron probe microanalysis

All tibiae were sectioned transversely using an Isomet diamond wafer saw (Buehler Ltd., Lake Bluff, IL, USA). The mineralized bone block encompassing the proximal epiphysis-metaphysis (the site of tumor cell injection) was defatted in acetone for 2 weeks then dried in a 40 °C oven and embedded in epoxy (Epo-Kwick®, Buehler Ltd.). Cylindrical molds (1 in. in diameter and height) were used with the bone embedded sagitally for fine grinding and polishing (~0.5 μm) on an automated lapping plate. Sample surfaces were then coated with 20-30 nm thickness carbon, and electron probe microanalysis (EPMA) was undertaken with a Cameca SX100 electron probe (Cameca, Paris FR), equipped with both Wavelength Dispersive Spectroscopy (WDS) and Energy Dispersive Spectroscopy (EDS), using vendor supplied PeakSight 4.1 (Cameca, Paris, France) analysis software. Elemental calcium (Ca) Kα and phosphorus (P) Kα were analysed in the same bony regions under 2 μm resolution, 15 kV and 15 nA. The generated map size for one unit was 512 × 512 pixels as 1 mm × 1 mm. Apatite_639 [$Ca_5(PO_4)_3F$] standards were used to standardize subsequent quantitative analyses. PeakSight 4.1 software was employed to calculate elemental Ca and P weight percent against a reference spectrum, in order to measure both distribution and concentration.

5.17. Mercuric chloride staining

Representative limbs from each group were stained by immersion in 5% Mercury (II) chloride ($HgCl_2$) for 24 h to improve soft tissue contrast and imaged with conventional micro-CT at 18 μm resolution,. Tumor tissue volume was represented using SkyScan-bundled Data Viewer software, with greyscale tissue densities represented in different colours using a preset thresholding range, with adipose tissues shown in blue, and hydrophilic muscle and solid tumor tissues represented in the warmer green, yellow and red colours with increasing density respectively.

5.18. Statistical analysis

Results are presented as mean ± standard deviations. Statistical significance was determined using one way or two-way analysis of variance or a *t*-test. A $p < 0.05$ was taken to indicate significance for all assays. Individual number of replicates (n) for each study is given in the captions to all relevant figures.

Supplementary data to this article can be found online at https://doi.org/10.1016/j.bone.2019.04.014.

Acknowledgements

The authors acknowledge the help of Drs Beng Chu and Tara Pike, and Ms. Kodee King of the Curtin University Life Sciences Testing Facility. Curtin University Academic50 funds and Victoria University Collaborative Research Grant Scheme were used for this project with no influence on the study by the governing funding bodies. Apart from these, this body of research did not receive any specific grant from funding agencies in the public, commercial, or not-for-profit sections.

Dedication

This study is dedicated to the loving memories of Mrs. Manorma Devi (Maa), Mrs. Tulsiamma Rao (Nani), and Mrs. Ramraji Rattan (Aji).

References

[1] F. Camnasio, C. Scotti, G.M. Peretti, F. Fontana, G. Fraschini, Prosthetic joint replacement for long bone metastases: analysis of 154 cases, Arch. Orthop. Trauma Surg. 128 (2008) 787–793.
[2] E.S. Rosa Mendoza, E. Moreno, P.B. Caguioa, Predictors of early distant metastasis in women with breast cancer, J. Cancer Res. Clin. Oncol. 139 (2013) 645–652.
[3] S. Casimiro, K.S. Mohammad, R. Pires, J. Tato-Costa, I. Alho, R. Teixeira, A. Carvalho, S. Ribeiro, A. Lipton, T.A. Guise, L. Costa, RANKL/RANK/MMP-1 molecular triad contributes to the metastatic phenotype of breast and prostate cancer cells in vitro, PLoS One 8 (2013) e63153.
[4] H. Lee, K.L. Sodek, Q. Hwang, T.J. Brown, M. Ringuette, J. Sodek, Phagocytosis of collagen by fibroblasts and invasive cancer cells is mediated by MT1-MMP, Biochem. Soc. Trans. 35 (2007) 704–706.
[5] K. Holmbeck, P. Bianco, S. Yamada, H. Birkedal-Hansen, MT1-MMP: a tethered collagenase, J. Cell. Physiol. 200 (2004) 11–19.
[6] J.A. Doll, V.M. Stellmach, N.P. Bouck, A.R. Bergh, C. Lee, L.P. Abramson, M.L. Cornwell, M.R. Pins, J. Borensztajn, S.E. Crawford, Pigment epithelium-derived factor regulates the vasculature and mass of the prostate and pancreas, Nat. Med. 9 (2003) 774–780.
[7] C. Ramirez-Castillejo, F. Sánchez-Sánchez, C. Andreu-Agulló, S.R. Ferrón, J.D. Aroca-Aguilar, P. Sánchez, H. Mira, J. Escribano, I. Fariñas, Pigment epithelium-derived factor is a niche signal for neural stem cell renewal, Nat. Neurosci. 9 (2006) 331–339.
[8] C. Andreu-Agullo, J.M. Morante-Redolat, A.C. Delgado, I. Fariñas, Vascular niche factor PEDF modulates notch-dependent stemness in the adult subependymal zone, Nat. Neurosci. 12 (2009) 1514–1523.
[9] M. Yokoi, S. Yamagishi, M. Takeuchi, T. Matsui, Y. Yoshida, K. Ohgami, T. Amano-Okamoto, S. Ohno, Positive correlation between vitreous levels of advanced glycation end products and vascular endothelial growth factor in patients with diabetic retinopathy sufficiently treated with photocoagulation, Br. J. Ophthalmol. 91 (2007) 885–887.
[10] E.T. Ek, C.R. Dass, K.G. Contreras, P.F. Choong, Inhibition of orthotopic osteosarcoma growth and metastasis by multitargeted antitumor activities of pigment epithelium-derived factor, Clin Exp Metastasis 24 (2007) 93–106.
[11] P.X. Lee, J. Martinez, C.R. Dass, Stimulation of bone regeneration with pigment epithelium-derived factor microparticles: evidence in silico, in vitro and in vivo, Pharmazie 71 (2016) 382–389.
[12] S.P. Becerra, V. Notario, The effects of PEDF on cancer biology: mechanisms of action and therapeutic potential, Nat. Rev. Cancer 13 (2013) 258–271.
[13] R. Jan, M. Huang, J. Lewis-Wambi, Loss of pigment epithelium-derived factor: a novel mechanism for the development of endocrine resistance in breast cancer, Breast Cancer Res. 14 (2012) R146, https://doi.org/10.1186/bcr3356.
[14] C. Meyer, L. Notari, S.P. Becerra, Mapping the type I collagen-binding site on pigment epithelium-derived factor. Implications for its antiangiogenic activity, J. Biol. Chem. 277 (2002) 45400–45407.
[15] S. Mathews, S.A. Mathew, P.K. Gupta, R. Bhonde, S. Totey, Glycosaminoglycans enhance osteoblast differentiation of bone marrow derived human mesenchymal stem cells, J. Tissue Eng. Regen. Med. 8 (2014) 143–152.
[16] M.L. Broadhead, S.P. Becerra, P.F. Choong, C.R. Dass, The applied biochemistry of PEDF and implications for tissue homeostasis, Growth Factors 28 (2010) 280–285.
[17] G. Filiz, C.R. Dass, Reduction in tumour cell invasion by pigment epithelium-

derived factor is mediated by membrane type-1 matrix metalloproteinase down-regulation, Pharmazie 67 (2012) 1010–1014.
[18] M.L. Tan, P.F. Choong, C.R. Dass, Anti-chondrosarcoma effects of PEDF mediated via molecules important to apoptosis, cell cycling, adhesion and invasion, Biochem. Biophys. Res. Commun. 398 (2010) 613–618.
[19] V. Nicolin, R. Bortul, R. Bareggi, G. Baldini, B. Martinelli, P. Narducci, Breast adenocarcinoma MCF-7 cell line induces spontaneous osteoclastogenesis via a RANK-ligand-dependent pathway, Acta Histochem. 110 (2008) 388–396.
[20] D. Schramek, V. Sigl, J.M. Penninger, RANKL and RANK in sex hormone-induced breast cancer and breast cancer metastasis, Tr Endocrinol Metab 22 (2011) 188–194.
[21] T. Akiyama, C.R. Dass, Y. Shinoda, H. Kawano, S. Tanaka, P.F. Choong, PEDF regulates osteoclasts via osteoprotegerin and RANKL, Biochem. Biophys. Res. Commun. 391 (2010) 789–794.
[22] E.T. Ek, C.R. Dass, K.G. Contreras, P.F. Choong, Pigment epithelium-derived factor overexpression inhibits orthotopic osteosarcoma growth, angiogenesis and metastasis, Cancer Gene Ther. 14 (2007) 616–626.
[23] E.T. Ek, C.R. Dass, K.G. Contreras, P.F. Choong, PEDF-derived synthetic peptides exhibit antitumor activity in an orthotopic model of human osteosarcoma, J. Orthop. Res. 25 (2007) 1671–1680.
[24] L. Mirabello, R.J. Troisi, S.A. Savage, International OS incidence patterns in children and adolescents, middle ages and elderly persons, Int. J. Cancer 125 (2009) 229–234.
[25] R. Siegel, D. Naishadham, A. Jemal, Cancer statistics, 2013, CA Cancer J. Clin. 63 (2013) 11.
[26] H. Kennecke, R. Yerushalmi, R. Woods, M.C. Cheang, D. Voduc, C.H. Speers, T.O. Nielsen, K. Gelmon, Metastatic behaviour of breast cancer subtypes, J. Clin. Oncol. 28 (2010) 3271–3277.
[27] T.B. Dorff, N. Agarwal, Bone-targeted therapies to reduce skeletal morbidity in prostate cancer, Asian J Androl 20 (2018) 215–220.
[28] H.E. Zhau, Q. Li, L.W.K. Chun, Interracial differences in prostate cancer progression among patients from the United States, China and Japan, Asian J Androl 15 (2013) 705–707.
[29] R. Coleman, J.J. Body, M. Aapro, P. Hadji, J. Herrstedt, ESMO Guidelines Working Group, Bone health in cancer patients: ESMO clinical practice guidelines, Ann. Oncol. 25 (2014) 124–137.
[30] B. Erdogan, I. Cicin, Medical treatment of breast cancer bone metastasis: from bisphosphonates to targeted drugs, Asian Pac. J. Cancer Prev. 15 (2014) 1503–1510.
[31] N. Harbeck, M. Gnant, Breast cancer, Lancet 389 (2017) 1134–1150.
[32] M.L. Broadhead, C.R. Dass, P.F. Choong, Systemically administered PEDF against primary and secondary tumours in a clinically relevant osteosarcoma model, Br. J. Cancer 105 (2011) 1503–1511.
[33] M. Sowers, Pregnancy and lactation as risk factors for subsequent bone loss and osteoporosis, J Bone Mineral Res 11 (1996) 1052–1060.
[34] J.C. Clark, T. Akiyama, C.R. Dass, P.F. Choong, New clinically relevant, orthotopic mouse models of human chondrosarcoma with spontaneous metastasis, Cancer Cell Int. 10 (2010) 20, https://doi.org/10.1186/1475-2867-10-20.
[35] O. Tacar, P. Sriamornsak, C.R. Dass, Doxorubicin: an update on anticancer molecular action, toxicity and novel drug delivery systems, J. Pharm. Pharmacol. 65 (2013) 157–170.
[36] A.M. Meredith, C.R. Dass, Increasing role of the cancer chemotherapeutic doxorubicin in cellular metabolism, J. Pharm. Pharmacol. 68 (2016) 729–741.
[38] S.V. Anisimov, N.S. Christophersen, A.S. Correia, V.J. Hall, I. Sandelin, J.Y. Li, P. Brundin, Identification of molecules derived from human fibroblast feeder cells that support the proliferation of human embryonic stem cells, Cell Mol Biol Lett 16 (2011) 79–88.
[39] Y. Cao, T. Yang, C. Gu, D. Yi, Pigment epithelium-derived factor delays cellular senescence of human mesenchymal stem cells in vitro by reducing oxidative stress, Cell Biol. Int. 37 (2013) 305–313.
[40] D.W. Dawson, O.V. Volpert, P. Gillis, S.E. Crawford, H. Xu, W. Benedict, N.P. Bouck, Pigment epithelium-derived factor: a potent inhibitor of angiogenesis, Science 285 (1999) 245–248.
[41] J.E. Cade, J. Hanison, The pancreas, Anaesthesia and Intensive Care Medicine 18 (2017) 527–531.
[42] R. Carnagarin, A.M. Dharmarajan, C.R. Dass, PEDF attenuates insulin-dependent molecular pathways of glucose homeostasis in skeletal myocytes, Mol. Cell. Endocrinol. 422 (2016) 115–124.
[43] Y. Chen, R. Carlessi, N. Walz, V.F. Cruzat, K. Keane, A.N. John, F.X. Jiang, R. Carnagarin, C.R. Dass, P. Newsholme, Pigment epithelium-derived factor (PEDF) regulates metabolism and insulin secretion from a clonal rat pancreatic beta cell line BRIN-BD11 and mouse islets, Mol. Cell. Endocrinol. 426 (2016) 50–60.
[44] A.K. Gattu, A.L. Birkenfeld, Y. Iwakiri, S. Jay, M. Saltzman, J. Doll, P. Protiva, V.T. Samuel, S.E. Crawford, C. Chung, Pigment epithelium-derived factor (PEDF) suppresses IL-1β-mediated c-Jun N-terminal kinase (JNK) activation to improve hepatocyte insulin signaling, Endocrinolog 155 (2014) 1373–1385.
[45] R. Carnagarin, R. Carlessi, P. Newsholme, A.M. Dharmarajan, C.R. Dass, Pigment epithelium-derived factor stimulates skeletal muscle glycolytic activity through NADPH oxidase-dependent reactive oxygen species production, Int. J. Biochem. Cell Biol. 78 (2016) 229–236.
[46] Y. Zhang, Y. Li, Z. Liu, Q. Zhao, H. Zhang, X. Wang, P. Lu, H. Yu, M. Wang, H. Dong, Z. Zhang, PEDF regulates lipid metabolism and reduces apoptosis in hypoxic H9c2 cells by inducing autophagy related 5-mediated autophagy via PEDF-R, Mol. Med. Rep. 17 (2018) 7170–7176.
[47] C.R. Dass, E.T. Ek, K.G. Contreras, P.F. Choong, A novel orthotopic murine model provides insights into cellular and molecular characteristics contributing to human osteosarcoma, Clin Exp Metastasis 23 (2006) 367–380.
[48] G.M. Quan, J. Ojaimi, A.P. Nadesapillai, H. Zhou, P.F. Choong, Resistance of epiphyseal cartilage to invasion by osteosarcoma is likely to be due to expression of antiangiogenic factors, Pathobiology 70 (2002) 361–367.
[49] I. Kozhukharova, V. Zemelko, Z. Kovaleva, L. Alekseenko, O. Lyublinskaya, N. Nikolsky, Therapeutic doses of doxorubicin induce premature senescence of human mesenchymal stem cells derived from menstrual blood, bone marrow and adipose tissue, Int. J. Hematol. 107 (2018) 286–296.
[50] A. Tinel, J. Tschopp, The PIDDosome, a protein complex implicated in activation of caspase-2 in response to genotoxic stress, Science 304 (2004) 843–846.
[51] T. Panaretakis, E. Laane, K. Pokrovskaja, A.C. Björklund, A. Moustakas, B. Zhivotovsky, M. Heyman, M.C. Shoshan, D. Grandér, Doxorubicin requires the sequential activation of caspase-2, protein kinase Cdelta, and c-Jun NH2-terminal kinase to induce apoptosis, Mol. Biol. Cell 16 (2007) 3821–3831.
[52] G.R. Dahal, P. Karki, A. Thapa, M. Shahnawaz, S.Y. Shin, J.S. Lee, B. Cho, I.S. Park, Caspase-2 cleaves DNA fragmentation factor (DFF45)/inhibitor of caspase-activated DNase (ICAD), Arch. Biochem. Biophys. 468 (2007) 134–139.
[53] M. Mogi, A. Togari, Activation of caspases is required for osteoblastic differentiation, J. Biol. Chem. 278 (2003) 47477–47482.
[54] M. Elahy, M.R. Doschak, J.D. Hughes, S. Baindur-Hudson, C.R. Dass, Alginate bead-encapsulated PEDF induces ectopic bone formation in vivo in the absence of co-administered mesenchymal stem cells, Curr. Drug Targets 19 (2018) 467–478.
[55] B.X. Yan, Y.X. Zheng, W. Li, J.Q. Chen, J. Zhou, S.Q. Cai, M. Zheng, X.Y. Man, Comparative expression of PEDF and VEGF in human epidermal keratinocytes and dermal fibroblasts: from normal skin to psoriasis, Discov. Med. 25 (2018) 47–56.
[56] C.R. Dass, P.F. Choong, Sequence-related off-target effect of Dz13 against human tumor cells and safety in adult and fetal mice following systemic administration, Oligonucleotides 20 (2010) 51–60.
[57] M.L. Tan, P. Shao, A.M. Friedhuber, M. van Moorst, M. Elahy, S. Indumathy, D.E. Dunstan, Y. Wei, C.R. Dass, The potential role of free chitosan in bone trauma and bone cancer management, Biomaterials 35 (2014) 7828–7838.
[58] S. Manchun, C.R. Dass, K. Cheewatanakornkool, P. Sriamornsak, Enhanced anti-tumor effect of pH-responsive dextrin nanogels delivering doxorubicin on colorectal cancer, Carbohydr. Polym. 126 (2015) 222–230.
[59] C.R. Dass, A.P. Nadesapillai, D. Robin, M.L. Howard, J.L. Fisher, H. Zhou, P.F. Choong, Downregulation of uPAR confirms link in growth and metastasis of osteosarcoma, Clin Exp Metastasis 2005 (22) (2005) 643–652.
[60] H.T. Ta, C.R. Dass, I. Larson, P.F. Choong, D.E. Dunstan, A chitosan-dipotassium orthophosphate hydrogel for the delivery of doxorubicin in the treatment of osteosarcoma, Biomaterials 30 (2009) 3605–3613.
[61] H.T. Ta, C.R. Dass, I. Larson, P.F. Choong, D.E. Dunstan, A chitosan hydrogel delivery system for osteosarcoma gene therapy with pigment epithelium-derived factor combined with chemotherapy, Biomaterials 30 (2009) 4815–4823.
[62] M.L. Tan, A.M. Friedhuber, C.R. Dass, Co-nanoencapsulated doxorubicin and Dz13 control osteosarcoma progression in a murine model, J. Pharm. Pharmacol. 65 (2013) 35–43.
[63] M.B. Alcantara, N. Nemazannikova, M. Elahy, C.R. Dass, Pigment epithelium-derived factor upregulates collagen I and downregulates matrix metalloproteinase 2 in osteosarcoma cells, and colocalizes to collagen I and heat shock protein 47 in fetal and adult bone, J. Pharm. Pharmacol. 66 (2014) 1586–1592.
[64] P. Shao, Y. Wei, C.R. Dass, G. Zhang, Z. Wu, Systemic delivery of free chitosan accelerates femur fracture healing in rats, Curr. Drug Targets 19 (2018) 460–466.
[65] Z. Wu, P. Shao, C.R. Dass, Y. Wei, Systemic leptin administration alters callus VEGF levels and enhances bone fracture healing in wildtype and Ob/Ob mice, Injury 49 (2018) 1739–1745.
[66] T. Akiyama, C.R. Dass, Y. Shinoda, H. Kawano, S. Tanaka, P.F. Choong, Systemic RANK-fc protein therapy is efficacious against primary osteosarcoma growth in a murine model via activity against osteoclasts, J. Pharm. Pharmacol. 62 (2010) 470–476.
[67] C.R. Dass, P.F. Choong, Zoledronic acid inhibits osteosarcoma growth in an orthotopic model, Mol. Cancer Ther. (12) (2007) 3263–3270.
[68] X. Yu, L. Yang, M.J. Cairns, C. Dass, E. Saravolac, X. Li, L.Q. Sun, Chemosensitization of solid tumors by inhibition of Bcl-xL expression using DNAzyme, Oncotarget 5 (2014) 9039–9048.